FINAL
CL 01-1673

Rover Localization Results for the FIDO Rover

E. T. Baumgartner, H. Aghazarian, and A. Trebi-Ollennu

Science and Technology Development Section,
Jet Propulsion Laboratory,
California Institute of Technology, Pasadena, CA 91109

ABSTRACT

This paper describes the development of a two-tier state estimation approach for NASA/JPL's FIDO Rover that utilizes wheel odometry, inertial measurement sensors, and a sun sensor to generate accurate estimates of the rover's position and attitude throughout a rover traverse. The state estimation approach makes use of a linear Kalman filter to estimate the rate sensor bias terms associated with the inertial measurement sensors and then uses these estimated rate sensor bias terms to compute the attitude of the rover during a traverse. The estimated attitude terms are then combined with the wheel odometry to determine the rover's position and attitude through an extended Kalman filter approach. Finally, the absolute heading of the vehicle is determined via a sun sensor which is then utilized to initialize the rover's heading prior to the next planning cycle for the rover's operations. This paper describes the formulation, implementation, and results associated with the two-tier state estimation approach for the FIDO rover.

Keywords: rover localization, rover state estimation, Kalman filter, inertial measurement units

1. INTRODUCTION

The Field Integrated Design and Operations (FIDO) Rover[1,2] (shown in Figure 1) continues to serve as NASA/JPL's technology development rover in support of upcoming Mars surface exploration missions. As such, the FIDO rover has demonstrated capabilities in the areas of remote science, in-situ instrument placement, and autonomous surface navigation including hazard detection and avoidance techniques. The underlying approach for the accurate navigation of the rover with respect to both short-range science targets and long-range navigation waypoints is based on the rover's ability to produce state estimates of the vehicle's pose (position, heading and attitude) with respect to a specific coordinate frame. This paper describes the continued development of the FIDO rover localization approach that was previously presented in a paper by Baumgartner et al.[3] In particular, recent work has focused on the use of FIDO's inertial measurement unit (IMU) sensors for the estimation of the rover's orientation and attitude as the vehicle traverses from one site to another. The IMU consists of 3-axis accelerometers and 3-axis gyroscope rate sensors. This paper will describe the two-tier state estimation approach based around the Kalman filter. The lower-tier Kalman filter estimates the gyro bias terms while the rover remains in a stationary position. The rover's heading relative to a north-aligned reference frame is initialized using a rover-mounted sun sensor. As the vehicle traverses, the higher-tier Kalman filter then fuses wheel odometry and the output from the gyro-based Kalman filter. Finally, the rover updates its absolute heading information again with the on-board sun sensor. Extensive results from both the gyro-bias estimation technique and the state estimation results gathered during rover traverses are presented.

The primary framework for the FIDO rover localization approach is based on the work presented in Baumgartner and Skaar[4] and Yoder et al[5] that describes a time-independent extended Kalman filter formulation for the determination of the rover's state estimates. Many researchers have also studied the problem of integrating inertial measurement units on mobile robots for improved rover state estimation. These researchers include Barshan and Durrant-Whyte,[6] Vaganay et al,[7] Goel et al,[8] and Chung et al.[9] The IMU modeling approach presented in this paper closely matches the techniques described by Goel et al[8] and Chung et al.[9] Finally, this paper presents a novel approach for determining wheel odometry for an independently-driven 6 wheel drive rover system that improves dead-reckoning performance by synchronizing the closed-loop velocity control for each of the 6 drive wheels.

Section 2 details the state estimation framework for the propagation of the state estimates using wheel odometry and the update of the state estimates using the attitude measurements while Section 3 describes the state estimation

Send correspondence to E. T. Baumgartner, E-mail: Eric.T.Baumgartner@jpl.nasa.gov.

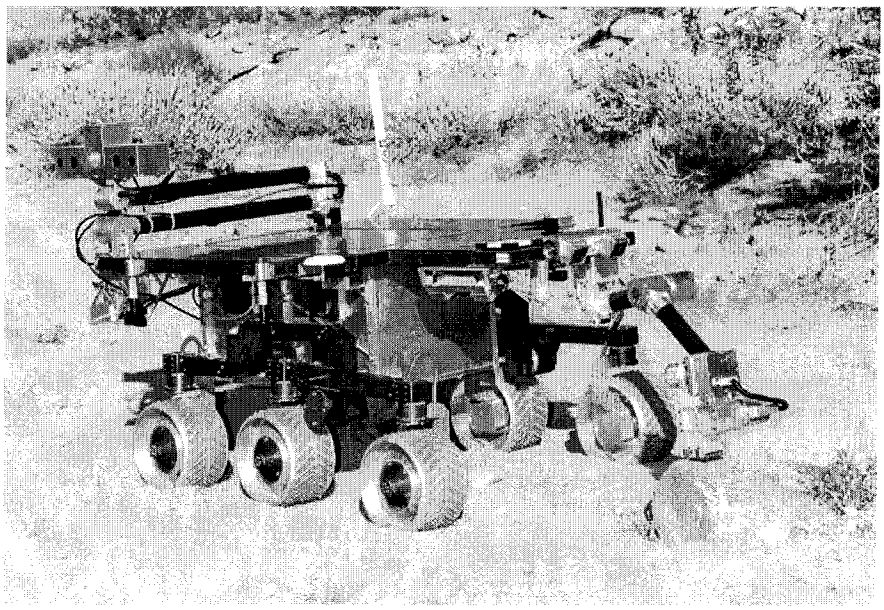

Figure 1. The FIDO rover with in-situ instrument arm extended.

technique that is utilized to estimate the rate sensor bias terms associated with the IMU. The means for generating the wheel odometry associated with the 6-wheel drive rover mobility system is described in Section 4. Experimental results from the IMU rate sensor bias estimator and from the rover's state estimator are presented in Section 5 and some concluding remarks are provided in Section 6.

2. ROVER STATE ESTIMATION

This section describes the generation of the rover state estimates based on the extended Kalman filter formulation originally described in Baumgartner and Skaar[4] and Baumgartner et al.[3] For the FIDO rover, the nominal vehicle motion consists of arc turns based on Ackerman steering, straight drives, or turn-in-place motions about the center of the vehicle. For these motions, the rover state is defined as the planar position of the rover, (X,Y), and the heading or yaw angle relative to a north-aligned reference frame, (ϕ), as shown in Figure 2.

For a Ackerman-based arc turns and for straight drives, the state equations that describe the motion of the rover based on wheel odometry alone are described by the following equations:

$$\frac{d\mathbf{x}(\alpha)}{d\alpha} = \begin{bmatrix} \frac{dX(\alpha)}{d\alpha} \\ \frac{dY(\alpha)}{d\alpha} \\ \frac{d\phi(\alpha)}{d\alpha} \end{bmatrix} = \begin{bmatrix} R\cos\phi(\alpha) \\ R\sin\phi(\alpha) \\ \frac{R}{B}u \end{bmatrix} + \mathbf{w}(\alpha) = \mathbf{f}(\mathbf{x}(\alpha), u) + \mathbf{w}(\alpha) \tag{1}$$

where $\mathbf{x} = [X\ Y\ \phi]^{\mathrm{T}}$, R is the nominal wheel radius, and B is half the distance between the wheel base. The independent variable, α, is defined as

$$\alpha = \frac{\theta_l + \theta_r}{2} \tag{2}$$

where θ_l and θ_r are the average absolute wheel rotations of the left and right side wheels, respectively. The control variable, u, is defined as

$$u = \frac{d\theta_l - d\theta_r}{d\theta_l + d\theta_r} \tag{3}$$

where $d\theta_l$ and $d\theta_r$ are the average differential wheel rotations of the left and right side wheels, respectively. The process noise, $\mathbf{w}(\alpha)$, is assumed to be a random process that captures the uncertainty in the state equations due to issues such as wheel slippage, etc.

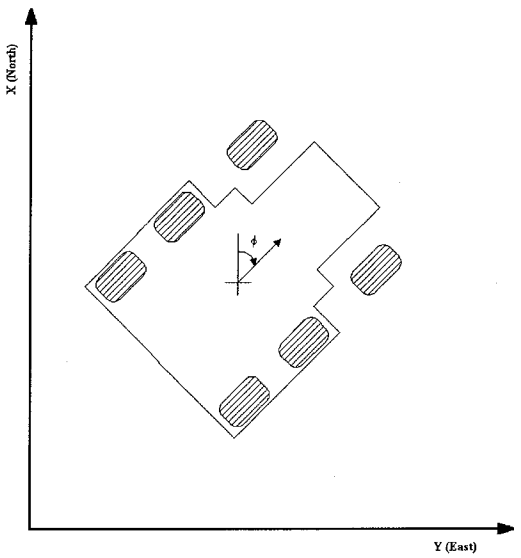

Figure 2. Rover coordinate frame.

The state equations given in Equation 1 are valid for all maneuvers except for a turn-in-place maneuver for which the independent variable, α, goes to zero and the state equations become singular. To handle this special case, α is re-defined as

$$\alpha = \frac{\theta_l - \theta_r}{2} \tag{4}$$

which results in the following state-equations for a turn-in-place maneuver:

$$\frac{d\mathbf{x}(\alpha)}{d\alpha} = \begin{bmatrix} \frac{dX(\alpha)}{d\alpha} \\ \frac{dY(\alpha)}{d\alpha} \\ \frac{d\phi(\alpha)}{d\alpha} \end{bmatrix} = \begin{bmatrix} 0 \\ 0 \\ \frac{R}{B} \end{bmatrix} + \mathbf{w}(\alpha) = \mathbf{f}(\mathbf{x}(\alpha)) + \mathbf{w}(\alpha) \ . \tag{5}$$

In either case, with the real-time sensing of the wheel rotations via wheel encoders, the above state equations are numerically integrated (e.g., propagated) in real-time thereby producing the dead-reckoned estimates of the rover motion.

Likewise, the estimation error covariance matrix, $\mathbf{P}(\alpha)$, associated with the extended Kalman filter is propagated in real-time by the following equation:

$$\frac{d\mathbf{P}(\alpha)}{d\alpha} = \mathbf{F}(\mathbf{x}(\alpha))\mathbf{P}(\alpha) + \mathbf{P}(\alpha)\mathbf{F}(\mathbf{x}(\alpha))^{\mathrm{T}} + \mathbf{Q} \tag{6}$$

where $\mathbf{F}(\mathbf{x}(\alpha))$ is the Jacobian of the state equations evaluated at the current value of the state and $\mathbf{Q}$ is the covariance matrix associated with the process noise. The process noise covariance matrix is assumed to be a diagonal matrix, i.e., $\mathbf{Q} = \mathrm{diag}[Q_{XX},\ Q_{YY},\ Q_{\phi\phi}]$, and, qualitatively, represents the confidence placed in the dead-reckoned estimates of the state.

The update equations associated with the extended Kalman filter are given by

$$\hat{\mathbf{x}}(\alpha^+) \ = \ \hat{\mathbf{x}}(\alpha^-) + \mathbf{K}(\alpha^+)[\mathbf{z}(\alpha^+) - \mathbf{h}(\hat{\mathbf{x}}(\alpha^-))] \tag{7}$$

where the Kalman gain, $\mathbf{K}(\alpha^+)$, is

$$\mathbf{K}(\alpha^+) \ = \ \mathbf{P}(\alpha^-)\mathbf{H}(\hat{\mathbf{x}}(\alpha^-))^{\mathrm{T}}[\mathbf{H}(\hat{\mathbf{x}}(\alpha^-))\mathbf{P}(\alpha^-)\mathbf{H}(\hat{\mathbf{x}}(\alpha^-))^{\mathrm{T}} + \mathbf{R}]^{-1} \tag{8}$$

and where, in Equations 7 and 8, α^+ represents the value of α when a new measurement is acquired and $\hat{\mathbf{x}}(\alpha^+)$ refers to the updated rover state. Also, in these equations, $\hat{\mathbf{x}}(\alpha^-)$ represents the propagated state estimates produced by integrating forward the state equations given either by Equation 1 or by Equation 5 assuming zero process noise. In Equation 8, $\mathbf{H}(\hat{\mathbf{x}}(\alpha^-))$ is the Jacobian of the measurement equation which is evaluated at the propagated value of the rover state. Finally, the measurement noise covariance matrix is denoted by $\mathbf{R}$. For this paper, the measurements represent either the output from the IMU's yaw rate sensor, ϕ_{imu}, or the sun sensor, ϕ_{sun}. In both cases, the measurement is a direct measure of the rover's heading. For the sun sensor, the heading measurement is an absolute heading relative to a north-aligned reference frame while, for the IMU, the heading measurement is relative to the previous position of the rover.

The estimation error covariance matrix is updated as follows

$$\mathbf{P}(\alpha^+) = [\mathbf{I} - \mathbf{K}(\alpha^+)\mathbf{H}(\hat{\mathbf{x}}(\alpha^-))]\mathbf{P}(\alpha^-) \tag{9}$$

where $\mathbf{I}$ is the 3×3 identity matrix and, in the above equation and in Equation 8, $\mathbf{P}(\alpha^-)$ represents the propagated estimation error covariance matrix produced by the integration of Equation 6.

3. RATE SENSOR BIAS ESTIMATION

For the IMU sensor, the attitude of the vehicle is described by the roll (r), pitch (p) and the yaw or heading (ϕ) angles where the yaw angle is defined in Figure 2 and the roll and pitch angles are specified relative to the local gravity vector about the rover's local X and Y coordinate frame axis, respectively. The roll and pitch angles of the rover are determined by the 3-axis accelerometer and the heading of the vehicle during motion is determined using the yaw gyroscope rate sensor.

When the rover is stationary, the IMU rate sensor bias terms are estimated via a linear Kalman filter based on the following state equations:

$$\frac{d\dot{r}_{bias}(t)}{dt} = 0 + w_{r_{bias}}(t) \tag{10}$$

$$\frac{d\dot{p}_{bias}(t)}{dt} = 0 + w_{p_{bias}}(t) \tag{11}$$

$$\frac{d\dot{\phi}_{bias}(t)}{dt} = 0 + w_{\phi_{bias}}(t) \tag{12}$$

and measurement equations:

$$\dot{r}_{bias}(t) = \dot{r}_{meas}(t) + v_{r_{bias}}(t) \tag{13}$$

$$\dot{p}_{bias}(t) = \dot{p}_{meas}(t) + v_{p_{bias}}(t) \tag{14}$$

$$\dot{\phi}_{bias}(t) = \dot{\phi}_{meas}(t) + v_{\phi_{bias}}(t)\ . \tag{15}$$

In the state equations, it is assumed that the rate sensor bias terms are slowly time-varying constants that are driven by process noise. For the measurement equations, since the rover is stationary, the measurement of the rate sensor bias is identical to the measured rate plus some measurement noise.

When the rover begins its motion, the rate sensor bias estimator is deactivated and the most recent rate sensor bias term is then used to integrate the yaw rate sensor measurements in real-time to determine the heading of the vehicle throughout the rover's traverse. During the rover motion, the IMU-based heading of the vehicle, $\phi_{imu}(t)$, is determined by

$$\phi_{imu}(t_i) = (\dot{\phi}_{meas}(t_i) - \dot{\phi}_{bias}(t_{init}))(t_i - t_{i-1}) + \phi(t_{i-1}) \tag{16}$$

where the bias term $\dot{\phi}_{bias}(t_{init})$ is calculated prior to the rover movement, the rate sensor term $\dot{\phi}_{meas}(t)$ are measured directly from the IMU during rover motion, and t_i represents the ith sampling time of the rate sensor.

This overall approach to the integration of the rate sensor information to produce rover yaw/heading information is predicated on the assumption that the rover navigates in moderate increments in both position and orientation such that the rate sensor bias estimation can be reactivated after motion of the rover. For example, FIDO's autonomous hazard detection and navigation algorithm increments the rover's position in 1 meter steps and variable angle turns

separated by hazard detection using stereo ranging sensors at which time the rover is stationary. Therefore, while the rate sensor bias terms may drift over long time durations, the ability to quickly re-estimate these bias terms every time the rover becomes stationary after a traverse allows us to treat the rate sensor bias terms as slowly time-varying constants.

4. WHEEL ODOMETRY FOR A 6-WHEEL ROVER

NASA/JPL has utilized the rocker-bogie suspension system with 6 independently driven and steered wheels for the design of many planetary rovers including the Sojourner rover[10] and the FIDO rover.[11] This passive suspension system represents a compact mechanism that has the ability to safely traverse over obstacles that are up to 1.5 times the rover's wheel diameter. As the rover drives and the rocker-bogie suspension system conforms to the terrain topography, each of the 6 wheels experience a different loading profile that, in some configurations, causes the wheels to "fight" one another. In other words, as each wheel is controlled in a closed-loop manner such that the wheel drive follows its own separate velocity profile, the interaction between each wheel as it encounters a different loading condition may result in one wheel speeding up to meet its commanded velocity set point while another wheel may be slowing down to meet its velocity set point. As such, all 6 wheels are traveling at different velocities relative to the commanded velocity set point. This results in an increased power requirement to drive the rover, excessive wheel slippage, and the tendency to side-slip as the suspension system traverses over obstacles. To minimize the effect of the wheels fighting one another, a velocity synchronization algorithm has been developed for the FIDO rover.

The first step in the velocity synchronization algorithm is outlier detection that determines which of the 6 wheels are deviating significantly from the closed-loop position along the nominal velocity profile. Let θ_m equal the distance traveled by the m^{th} wheel for $m = 1, \ldots, 6$, then the deviation of the distance traveled by one wheel relative to the distance traveled by all other wheels is given by

$$\Delta_m = \sum_{i=1, i \neq m}^{6} |\theta_m - \theta_i| \tag{17}$$

for $m = 1, \ldots, 6$. The average of the deviation is:

$$\Delta_{avg} = \frac{1}{6} \sum_{i=1}^{6} \Delta_m \ . \tag{18}$$

A voting scheme is then utilized to determine a composite score associated with those wheels that are closely matched to one another. In other words, the composite score seeks to identify the outliers and not include these outliers in the average distance associated with the non-outlier wheels. The composite score, S, is determined by the following equation:

$$S = \sum_{m=1}^{6} \begin{cases} \theta_m & \text{if } \Delta_m \leq \Delta_{avg} \\ 0 & \text{otherwise} \end{cases} \tag{19}$$

where a counter, c, is incremented each time $\Delta_m \leq \Delta_{avg}$ is encountered in Equation 19. Finally, the voted average wheel distance is computed as $\theta_{vote} = S/c$.

The last step in the velocity synchronization algorithm is the computation of the required change in the commanded velocity set point relative to the nominal velocity set point for the m^{th} wheel, V_m, according to the following equations:

$$\delta_m = \theta_{vote} - \theta_m \tag{20}$$

$$V_m = V_{nominal} + \Delta_V \tag{21}$$

where

$$\Delta_V = \begin{cases} \delta_m V_{nominal} & \text{if } \delta_m V_{nominal} \leq \Delta V_{threshold} \\ \Delta V_{threshold} & \text{otherwise} \end{cases} \tag{22}$$

and where, in Equation 21, $V_{nominal}$ represents the nominal velocity set point for each of the wheels and, in Equation 22, $\Delta V_{threshold}$ represents the limit or dynamic range associated with how large of a velocity change can be accommodate by the closed-loop control system.

As a result of this velocity synchronization approach, the power required to drive the 6-wheeled FIDO rover is significantly reduced when compared to the power required when a tight, non-synchronized, closed-loop control approach. Through several experiments associated with assessing the rover's driving performance in a variety of terrain settings, wheel slippage is minimal and all 6 wheels start and end their motion at the same time. Finally, the resulting voted wheel distance, θ_{vote}, for the right and left side wheels is utilized as the means for determining the values of α and u as in Equations 2 and 3, respectively.

5. RESULTS

In this section, the results from the IMU bias estimation work are presented along with rover state estimation results from the most recent FIDO field test near the Soda Mountains in the California's, Mojave Desert. The FIDO rover carries a 266 MHz, Pentium-class CPU which runs the VxWorks 5.4 real-time operating system. All software for the FIDO rover is written in ANSI-C and is structured according to a three-layer architecture with the layers known as the driver layer, the device layer, and the application layer. All hardware dependencies are handled in the driver layer. The middle device layer provides the means for abstracting the higher level software in the application layer from the hardware dependencies. The device layer is responsible for all motion control functions, vision processing, instrument interfaces, forward and inverse kinematics for the rover and rover-mounted robot arms, etc. The application layer contains all rover sequences, instrument sequences, hazard detection and avoidance software, etc.

As stated previously, the FIDO rover is a independently-controlled 6-wheel drive and steer vehicle with a passive rocker-bogie suspension system. Each wheel actuator is outfitted with a quadrature optical encoder that can resolve the rotation of a wheel to within 0.027 degrees which corresponds to a incremental wheel travel of 0.0485 mm for the 20 cm diameter wheels on FIDO. All encoder data on the rover is collected at 200 Hz and utilized at 50Hz as the feedback sensor for the closed-loop PID velocity and PID position control of all of the rover's actuators. At the 50 Hz data rate, the propagation equations given in Equations 1 or 5 are integrated to produce the propagated state estimates assuming zero process noise. The velocity synchronization approach described in Section 4 runs at the 10 Hz rate.

The sun sensor on the FIDO rover consists of a CCD imager with a wide field-of-view lens (approximately 110 degrees) that is includes a neutral density filter in the optical path. The centroid of the sun is determined using a thresholding and centroid finding algorithm with outlier rejection. Given the location of the sun in the 2D image plane of the CCD sensor, a ray vector from the sun sensor to the sun is determined through knowledge of the internal camera parameters. The sun sensor camera is modeled as a fish-eye camera/lens system[12] and the set of 21 camera parameters associated with this camera model are determined using a calibration procedure. With the ray vector to the sun determined with respect to the sun sensor frame, the ray vector is then transformed to a gravity-down rover reference frame using IMU's accelerometers. From the ray vector with respect to the rover frame along with knowledge of where the sun should appear in the sky given time of day and the position of the rover on the Earth's surface (latitude and longitude), the heading of the rover with respect to a north-aligned reference frame, ϕ_{sun}, is determined. Additional details concerning the FIDO sun sensor can be found in Trebi-Ollennu, et al.[13]

FIDO also carries a commercial three axis accelerometer and gyroscope IMU package. The rate sensors consist of vibrating ceramic plates that utilize the Coriolis force to output angular rate information that is independent of acceleration and the accelerometers are surface micro-machined silicon devices that use differential capacitance to sense acceleration.[14] The IMU package on FIDO has a rate sensor range of ± 50 degrees per second and a sensitivity of approximately 25 degrees per second per volt. The range for the accelerometers is ± 2 g's with a sensitivity of approximately 1 g per volt. The interface to the unit is either through a RS232 serial link or via a direct analog output from the IMU unit. Data from the IMU is collected at a sampling rate of 200 Hz.

The overall state estimation approach utilized during the recent FIDO rover field test is shown in Figure 3. This figure indicates that the rate sensor bias estimation occurs whenever the rover is stationary. During rover motion, the latest bias estimate is utilized to determine the IMU-based heading of the vehicle as well as the integration of the rover state equations to yield the dead-reckoned estimates of the state. When the rover ends its motion, the IMU-based heading is fused together with the dead-reckoned estimates of the state using the technique outlined in Section 2. During autonomous navigation of the rover, the vehicle stops for 30 seconds approximately every 1 meter to conduct hazard detection based on stereo imaging. While the rover is stationary, the rate sensor bias estimator is re-engaged to compute the bias terms. At the end of a traverse, the absolute heading of the vehicle is updated using the sun sensor. This absolute heading is then used for the next rover planning cycle.

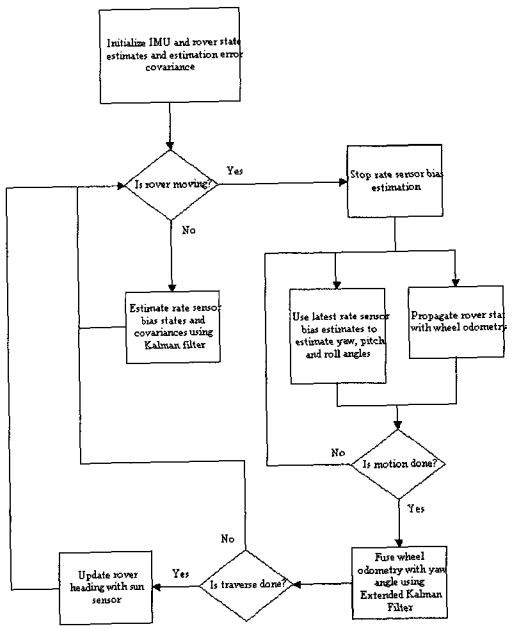

Figure 3. Rover state estimation block diagram.

To test the IMU rate sensor bias estimation technique, data was collected from the FIDO's IMU for approximately 10 minutes while the rover remained stationary. Nine separate data sets were collected on different days at different times so that the temperature of the IMU varied for each of the data sets. Two of the nine data sets including the results from the rate sensor bias estimation technique are presented in this paper. The bias estimator operates on the IMU data at 200 Hz (the same rate as the IMU sampling). Results from these two data sets are shown in Figure 4 and Figure 5. In these two data sets, the filter converges rapidly within 0.5 seconds from the start of the run as indicated in Figures 4(b) & (c) and 5(b) & (c). Also due to the collection of the data sets at different days and times, the rate sensor bias terms converge to different values (approximately 0.01 degrees per second for the first case and -0.02 degrees per second in the second case). Despite the different values for the estimated rate sensor bias terms, the estimate of the yaw angle using Equation 16 remains quite stable when compared to the rate sensor integration without bias estimation as shown in Figures 4(d) and 5(d).

To test the absolute accuracy of the state estimation approach described in this paper, the FIDO rover was placed in the rover pit located in JPL's Planetary Robotics Laboratory. This rover pit measures 9.1 $\times$ 4.5 meters^2 and is filled with a soft sand material and populated with a variety of rock type and sizes. Since the rover pit is located within an indoor environment, all elements of the rover localization approach shown in Figure 3 were utilized with the exception of the initialization of the rover heading using the sun sensor. The rover was commanded to follow a box trajectory which is 1 meter on a side and ended back at the initial starting position. The initial position of the rover was marked in the sand and the rover was commanded to follow the box trajectory. Throughout the traverse, the rover corrects its position and heading based on the two-tier state estimator. When the rover has reached the end of its trajectory, the error between the rover's end position relative to its starting position is measured physically with a ruler. This run was repeated 5 times with both the accumulated estimation error and the estimation error relative to the start of each run being recorded. The results of this run are shown in Figures 6 and 7. Figure 6 plots the rover state estimates that were generated during the traverse relative to the nominal box trajectory (indicated by the solid line with the $\times$ mark at the corners). The measured estimation error relative to the start of each box trajectory run is shown in Figure 7. For these 5 runs, the average of the absolute value of the error is 2.7 centimeters in the X direction and 2.0 centimeters in the Y direction over the 4 meter traverse associated with each box trajectory. These results correspond to a 0.84% error as a function of rover traverse distance. The overall accumulated error associated with all of the runs relative to the initial starting position for the first run is 13.5 centimeters in the X direction and -5.0 centimeters in the Y direction over the entire 20 meter traverse distance which corresponds to a

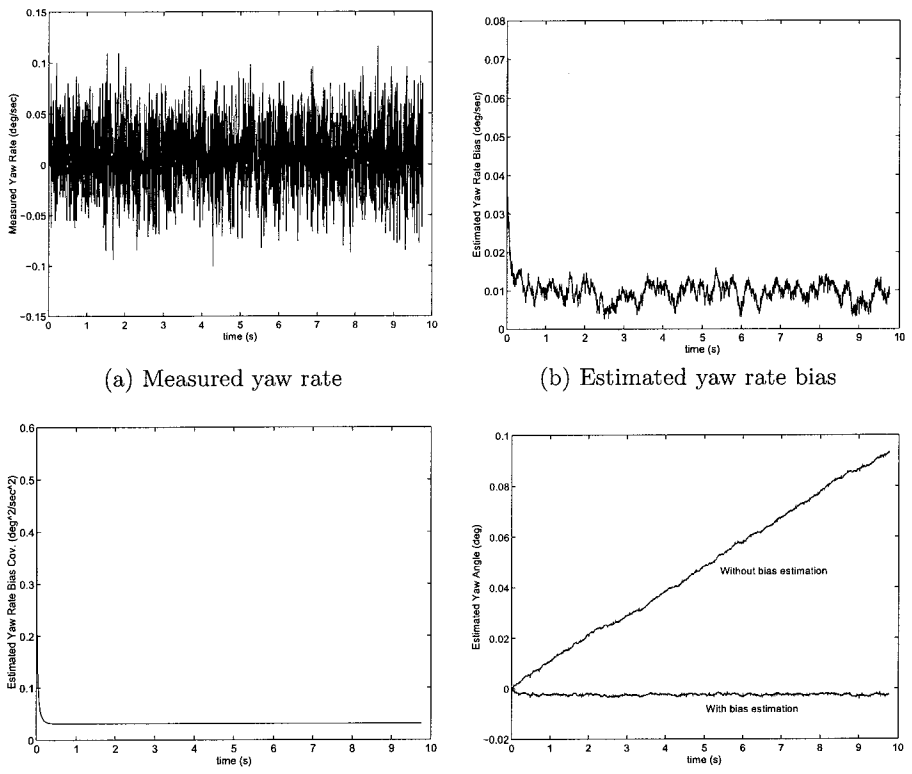

(a) Measured yaw rate

(b) Estimated yaw rate bias

(c) Estimated yaw rate error covariance

(d) Estimated yaw angle

Figure 4. Rate sensor bias estimation results — first data set.

0.72% error as a function of rover traverse distance.

The entire state estimation approach presented in this paper was also tested as a part of a full-scale FIDO rover field test in April/May 2001. The objectives of this test included the operation of the rover by a remote science and engineering team sequestered at JPL. The field test was conducted using a set of flight rules that will be observed during the upcoming NASA/JPL Mars Exploration Rover (MER) mission[15] that will land two rovers on the Martian surface in 2004. Such flight rules included operations planning times, downlink telemetry volume constraints, time and power constraints on rover operations. The FIDO rover was placed at a simulated "landing" site in a remote site near the Soda Mountains in California's Mojave Desert. The rover conducted remote sensing operations with its panoramic imaging systems and collected rock and soil compositional information using a near-infrared reflectance point spectrometer. With the identification of interesting scientific targets by the ground science team, the rover traversed to these targets using both an autonomous hazard detection/avoidance navigation technique as well as ground-directed rover moves. In particular, the rover was commanded to approach science targets such that the targets were located within the dexterous workspace of a robotic arm mounted on the rover. Typically, the rover is required to approach science targets to within ± 10 centimeters in position and ± 2 degrees in orientation in order for the in-situ instruments located on the end-effector of the robot arm to be capable of reaching the science target on the next set of operations. These required operations are therefore completely dependant on maintaining accurate estimates of the rover's position and attitude during traverses.

Figure 8 shows the state estimation results for the FIDO rover that were achieved during the 2001 FIDO/MER field test. In Figure 8, an aerial view of the field site is shown and the rover traverse is projected onto this view where the rover state estimation approach described in this paper provided the means for localizing the rover within this aerial view. The image shown in Figure 8(a) is a 7 km $\times$ 7 km area with the white box outlining the local area in which the rover operated. In Figure 8(b), the close-up aerial view, which encompases approximately a 1 km $\times$ 1 km area, shows the rover traverse by the black line in the image. The FIDO rover carries a differential GPS unit

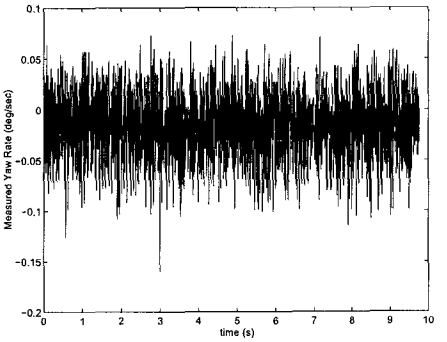

(a) Measured yaw rate

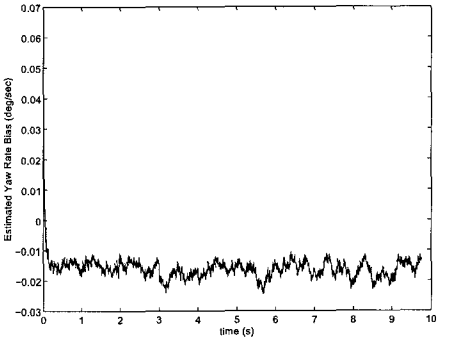

(b) Estimated yaw rate bias

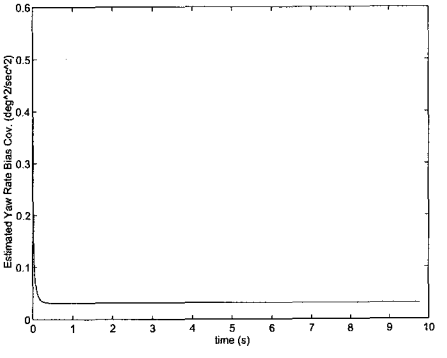

(c) Estimated yaw rate error covariance

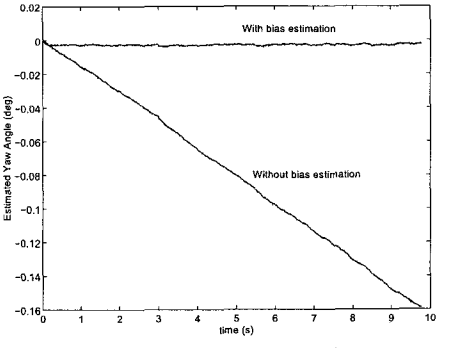

(d) Estimated yaw angle

Figure 5. Rate sensor bias estimation results — second data set.

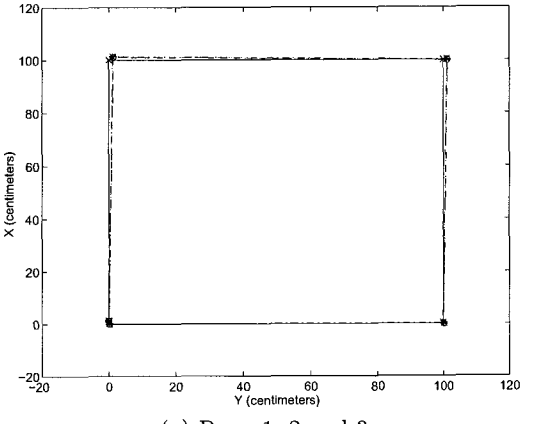

(a) Runs 1, 2 and 3

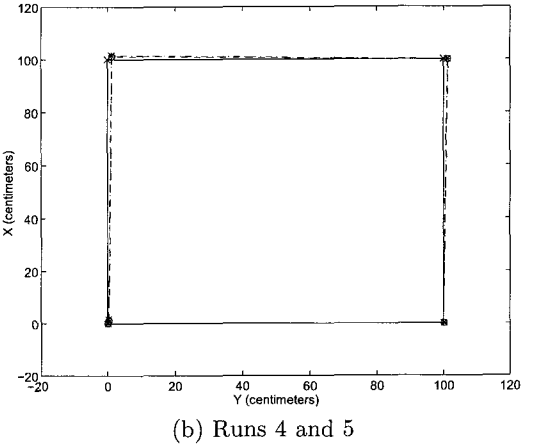

(b) Runs 4 and 5

Figure 6. State estimation results from box trajectory runs.

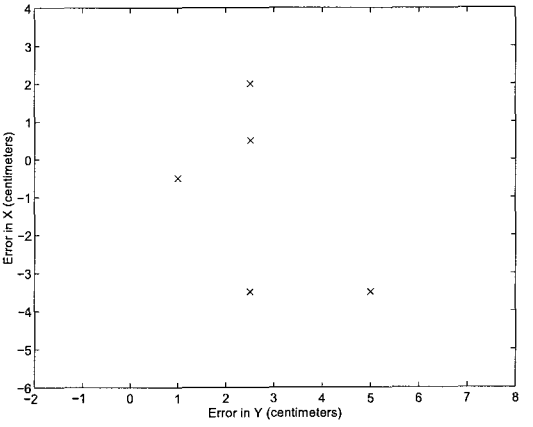

Figure 7. Measured final state estimation error for the 5 box trajectory runs.

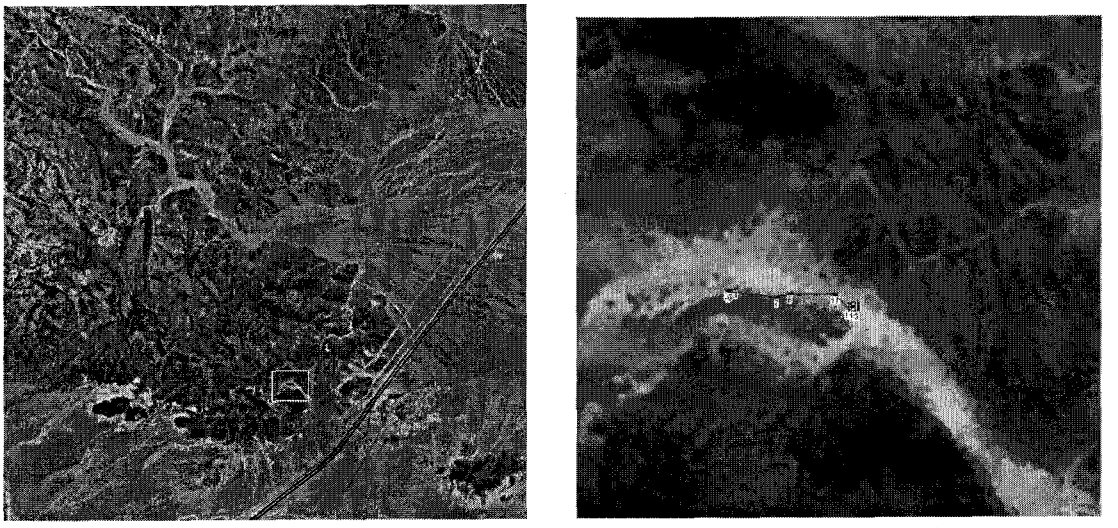

(a) Aerial view (7km×7 km) of field trial site (b) Close-up aerial view (1km×1km) of field trial site

Figure 8. Rover state estimation during the MER/FIDO field test.

for ground truthing purposes, however, during this field test the GPS unit was unable to produce position data for the rover, so no ground truth data is available for this traverse. In total, the rover traversed 135 meters throughout this field site successfully navigated autonomously for the entire traverse distance. The terrain in which the rover traversed was representative of a narrow wash that typically was 10 meters across the wash at the most narrow point.

6. CONCLUSIONS

This paper has outlined the development of an integrated state estimation approach using wheel odometry, IMU-based rate and attitude sensors, and a sun sensor for absolute heading measurements. This approach utilizes a linear Kalman filter to estimate the rate sensor bias terms while the rover is motionless and an extended Kalman filter to fuse together the wheel odometry, integrated rate sensor output, and sun sensor to produce the overall rover state estimate. Results for the IMU-based rate sensor bias estimator are presented along with the rover state estimates associated with ground-truthing experiments as well as rover traverses accomplished during the 2001 FIDO/MER field test.

ACKNOWLEDGMENTS

The research described in this paper was carried out at the Jet Propulsion Laboratory, California Institute of Technology, under a contract with the National Aeronautics and Space Administration.

REFERENCES

1. E. T. Baumgartner, "In-situ exploration of mars using rover systems," *Proceedings of the AIAA Space 2000 Conference*, AIAA Paper 2000-5062, Long Beach, CA, September 2000.
2. P. S. Schenker, E. T. Baumgartner, R. A. Lindemann, H. Aghazarian, A. J. Ganino, G. S. Hickey, D. Q. Zhu, L. H. Matthies, B. H. Hoffman, and T. L. Huntsberger, "New planetary rovers for long-range mars science and sample return," *Proceedings of SPIE*, **3522**, pp. 2-15, Boston, MA, October 1998.
3. E. T. Baumgartner, H. Aghazarian, A. Trebi-Ollennu, T. L. Hunstberger, M. S. Garrett, "State estimation and vehicle localization for the FIDO rover," *Proceedings of SPIE*, **4196**, pp. 329-336, Boston, MA, November 2000.
4. E. T. Baumgartner and S. B. Skarr, "An autonomous vision-based mobile robot," *IEEE Transactions on Automatic Control*, **39**(3), pp. 493-502, March 1994.
5. J.-D. Yoder, E. T. Baumgartner, and S. B. Skaar, "Initial results in the development of a guidance system for a power wheelchair," *IEEE Transactions on Rehabilitation Engineering*, **4**(3), pp. 143-151, September 1996.
6. B. Barshan and H. F. Durrant-Whyte, "Inertial navigation sensors for mobile robots," *IEEE Transactions on Robotics and Automation*, **11**, pp. 328-342, June 1995.
7. J. Vaganay, M. J. Aldon, and A. Fourinier, "Mobile robot attitude estimation by fusion of inertial data," *Proceedings of the International Conference on Robotics and Automation*, pp. 277-282, Atlanta, GA, May 1993.
8. P. Goel, S. I. Roumeliotis, and G. S. Sukhatme, "Robust localization using relative and absolute position estimates," *Proceedings of the IEEE/RSJ International Conference on Intelligent Robots and Systems*, pp. 1134-1140, 1999.
9. H. Chung, L. Ojeda, and J. Borenstin, "Accurate mobile robot dead-reckoning with a precision-calibrated fiber-optic gyroscope," *IEEE Transactions on Robotics and Automation*," **17**(1), pp. 80-84, February 2001.
10. D. Bickler, "Roving over mars," *Mechanical Engineering*, pp. 74-77, April 1998.
11. R. Lindemann, L. Reid, and C. Voorhees, "Mobility sub-system for the exploration technology rover," 33rd Aerospace Mechanisms Symposium, Pasadena, CA, May 1999.
12. Y. Xiong and K. Turkowski, "Creating image-based VR using self-calibrating fisheye lens," *Proceedings of IEEE Conference on Computer Vision and Pattern Recognition*, pp. 237-243, June 1997.
13. A. Trebi-Ollennu, T. Huntsberger, Y. Cheng, E. T. Baumgartner, B. Kennedy, and P. S. Schenker, "Design and analysis of a sun sensor for planetary rover absolute heading detection," accepted for publication in *IEEE Transactions on Robotics and Automation*, also documented in NASA Technical Brief CR-2001-210800, February 2001.
14. Crossbow Technology, Inc., *DMU User's Manual*, 1999.
15. Mars Exploration Rover websites: http://mars.jpl.nasa.gov/mer/ and http://athena.cornell.edu/, 2001.